

Agglomerated non-porous silica nanoparticles as model carriers in polyethylene synthesis

Cedric du Fresne von Hohenesche^{a,*}, Klaus K. Unger^b, Thomas Eberle^c

^a *Institut de Science et d'Ingénierie Supramoléculaires, ISIS, 8, allée Gaspard Monge, F-67083 Strasbourg, France*

^b *Institut für Anorganische Chemie und Analytische Chemie, Johannes Gutenberg-Universität, Duesbergweg 10-14, D-55128 Mainz, Germany*

^c *Office of Technology, Merck KGaA, Frankfurter Strasse 250, D-64271 Darmstadt, Germany*

Received 13 August 2003; received in revised form 1 July 2004; accepted 8 July 2004

Available online 12 August 2004

Abstract

Non-porous submicron silica particles (250 and 500 nm) with high monodispersity were agglomerated to form spherical agglomerates via spray drying. As a binder, 25 nm sized monodisperse silica spheres were selected from a variety of colloidal systems including Levasil-type and Aerosil-type silica nanoparticles. The use of such binders led to an increase of the specific surface area of the agglomerated carriers. All materials were characterised by nitrogen sorption, mercury intrusion and scanning electron microscopy. The silica agglomerates, with highly defined geometrical and pore structural parameters, were employed as model carriers in the heterogeneous polymerization of ethylene using a conventional methylaluminoxane (MAO)/ η^5 -dicyclopentadienyl zirconiumdichloride metallocene catalyst system. The activity of these model carriers was evaluated, as was the influence of MAO impregnation on the carriers' physico-chemical properties. The activity of the presented catalyst systems depended heavily on the percentage of binder. Due to skin formation, high contents of binder resulted in agglomerates with a smoother, more rigid surface. These carriers did not fragment during polymerization, and displayed low catalytic activity. Less binder gave more readily fragmented agglomerates displaying higher catalytic activities. Despite their small specific surface areas in comparison to commercially available polymerization carriers, e.g. SYLOPOL 948 from W.R. Grace, these model carriers possess similar activities, with the polymerization process depending more on the geometrical and structural aspects of the beads rather than on their specific surface areas. © 2004 Elsevier B.V. All rights reserved.

Keywords: Colloidal silica; Agglomerates; Carrier; Heterogeneous catalysis; Polyethylene; Fragmentation

1. Introduction

Homogenous catalysts formed by group IV metallocenes and methylaluminoxane (MAO) are of great interest for olefin polymerization [1,2]. Such systems combine high activity with excellent stereospecificity in the polymerization of α -olefins and provide tailoring of the stereoregularity of polymers through ligand design at the transition metal center [3]. Nevertheless, in practice, modern industrial polymerization processes require a heterogeneous catalyst to circumvent reactor fouling [4] (polymer adhesion at reactor walls) and to

enable direct morphology control of the polymer products [5,6].

In contrast to the traditional understanding of catalysts, polyolefin catalysts (catalyst and co-catalyst) remain within the product following use. This offers a new number of new possibilities concerning polymer properties, including the formation of polymer nanocomposites [7–9]. Likewise, the disadvantage of catalyst loss can be compensated for by the possibility of the direct formulation of granulates within the polymerization reactor. In order to obtain a clear, colorless material (e.g. for film application) without degrading the mechanical properties of the polymer, both the active catalyst and the carrier particles must be uniformly distributed during the polymerization process following carrier fragmentation (Fig. 1).

* Corresponding author. Tel.: +33 390 245178; fax: +33 390 245115.
E-mail address: cdfresne@isis.u-strasbg.fr (C.d.F. von Hohenesche).

Nomenclature

a_s	specific surface area according to BET
BET	Brunauer, Emmet and Teller
v_p	specific pore volume
p_d	mean pore diameter
d_p	particle diameter
$\rho_{\text{app(He)}}$	apparent density according to helium
A	polymerization activity
MAO	methyl aluminumoxane
M25	Monospher 25
M250	Monospher 250
M500	Monospher 500
TIBA	triisobutyl aluminum
PMMA	poly(methyl methacrylate)

In recent papers, a variety of supports, such as SiO_2 , Al_2O_3 [10], zeolites [11,12], Montmorillonite [13], etc. have been used. It has been established that porous, high surface area silica particles are preferable as carriers. Based on spherical silica, Fink and co-workers [14,15] performed thorough kinetic studies, correlated with microscopic visualization, in order to determine the specific mechanism of materials formation during heterogeneous olefin polymerization [16] (see Fig. 2). The break-up of the support during polymer formation was divided into three phases:

1. The induction period, where the olefin monomer is polymerized at the outer surface of the carrier, creating a diffusion barrier.
2. Polymer growth, accompanied by the fragmentation of the support.
3. Expansion of the polymer particle.

Unfortunately, little is known about the relationships between the physical features of the carrier (morphology, particle size, size and pore uniformity, surface area, etc.) and polymerization parameters like activity, molecular weight, molecular weight distribution and the granulate size of the polymer.

Here, a new approach involving tailor-made carriers is presented. We report on the synthesis, characterisation and application of a model carrier for the polymerization of olefins. In order to emphasize the influence of the support material on the polymerization behaviour and the properties of the final product rather than exploring new metallocene catalysts, an established system catalyst system was chosen (cyclopentadienyl zirconiumdichloride/methylaluminoxane/triisobutyl aluminium), with ethylene as the olefin monomer. Existing carrier systems consist mostly of irregularly shaped particles with rather disordered pore systems and pores of different dimensions and morphologies. In addition, the primary particles that make up these carriers generally possess a broad particle size distribution. Therefore, we focused on the construction of polymerization carriers by spray drying of highly monodisperse spherical primary particles with defined particle sizes and narrow size distributions.

2. Results

Fig. 1 depicts the scheme of carrier treatment, catalyst formation and olefin polymerization as conducted in this work. The polymer synthesis comprises several steps, including:

- Synthesis of the support material;
- Grafting of the MAO reagent onto the carrier surface;
- Metallocene impregnation of the carrier;
- Slurry polymerization of the olefin monomer.

The goal of this study was the construction of a model support with a spherical morphology and well-defined pores.

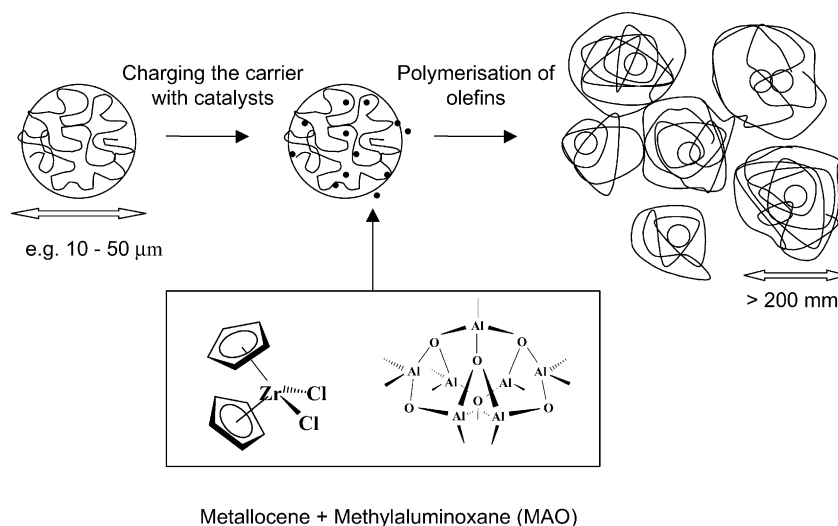


Fig. 1. Scheme of carrier treatment, catalyst formation and ethylene polymerization.

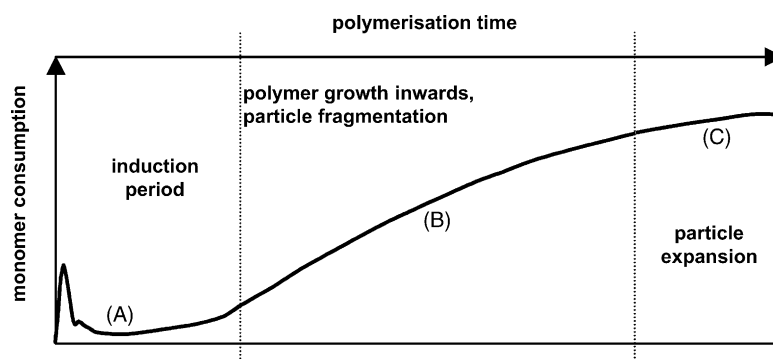


Fig. 2. Stages of supported metallocene-catalysed polymerization of olefins according to [16].

2.1. Agglomeration of colloidal particles

In order to achieve a homogeneous distribution and a defined fragmentation size of the support material in the polymer after polymerization, we chose a variety of silica colloids (Table 1). The particle sizes of the colloidal systems ranged from 7 to 500 nm and were products of Bayer AG (H.C. Starck), Germany (Levasil), Degussa AG, Germany (Aerosil) and Merck KGaA, Germany (Monospher). The Monospher materials were synthesized via a sol–gel process [17], more specifically via the well documented procedure of Stöber et al. [18], as modified by Giesche [19,20] to obtain fully dense silica colloids with particle sizes tuneable between 20 and 10 μm and with very narrow particle size distributions (less than 5% relative standard deviation). Monospher particles with diameters of 25, 250 and 500 nm (further referred to as M25, M250 and M500) were made available in large quantities for this work.

The colloidal systems presented in Table 1 were agglomerated via the spray drying technique. For this, the colloidal particles were dispersed in water and large agglomerates were obtained by fast evaporation of the water after droplet formation at the spray drying nozzle. The resulting particles were examined by nitrogen sorption, mercury intrusion and scan-

ning electron microscopy to assess pore structural parameters and morphological information, respectively. The influence of spray drying parameters on the spherical morphology of the agglomerated products, the agglomerate size and stability is qualitatively summarised in Table 2.

2.1.1. Pore structural parameters of agglomerated colloids

The data in Table 3 show that the specific surface areas reported by the manufacturers tended to be slightly higher than the values measured in this study. This could be explained by the loss of surface area due to inter-particle contacts within the agglomerate (neck formation). In general, the specific surface area of non-porous particles is purely geometrical and can be calculated according to Eq. (1).

$$a_s = \frac{6}{d_p \rho_{\text{app}}(\text{He})} \quad (1)$$

where a_s , specific surface area; d_p , particle diameter; $\rho_{\text{app}}(\text{He})$, apparent density of the material (as measured with helium).

According to theory, the mean pore diameter, being the inter-particle void volume of the agglomerated colloids, should depend on the type of packing and the particle dimensions [21,22], e.g. the pore diameter increases with increasing particle diameter and decreasing surface area. The porosity (pore volume and pore diameter) introduced by the agglomeration process depended on the initial particle dimensions of the colloidal system. Fig. 3 shows the dependence of the mean pore diameters of spray dried Levasil, Aerosil and Monospher dispersions on the initial particle size. It is clearly seen that with similar specific surface areas (and therefore, similar primary particle dimensions), the agglomerated Aerosils generated much larger pores. This can be explained by considering the agglomerated state of the Aerosil prior to our agglomeration via spray drying [23,24]. Transmission electron micrographs (not shown) revealed that the pores in agglomerated Aerosil were formed by cavities between pre-agglomerated nanoparticles, explaining the high pore volumes of the agglomerated Aerosil as well. In contrast, agglomerated Levasil and Monospher colloids consisted of a dense packing of nanoparticles without any pre-agglomeration, as indicated

Table 1
Characteristics of silica colloids used (manufacturer data)

Colloidal system		Specifications	
Product	Supplier	Mean particle-diameter, d_p (nm)	Specific surface area, a_s ($\text{m}^2 \text{g}^{-1}$)
Levasil 50	Bayer AG	~75	50
Levasil 100	Bayer AG	~30	100
Levasil 200	Bayer AG	~15	200
Levasil 300	Bayer AG	~9	300
Levasil 50S1	Bayer AG	~100	No data
Levasil 50S2	Bayer AG	~200	No data
Aerosil 90	Degussa AG	~20	90
Aerosil 200	Degussa AG	~12	200
Aerosil 300	Degussa AG	~7	300
Monospher 25	Merck KGaA	25	120
Monospher 250	Merck KGaA	250	12
Monospher 500	Merck KGaA	500	6

Table 2

Influence of spray drying parameters on the quality of agglomerate morphology, size and stability, based on SEM investigations of the agglomerates (↑: positive influence; ↓: negative influence; →: no influence; ↑↓: no strict correlation)

Increasing parameter	Influence on		
	Spherical morphology	Agglomerate size	Agglomerate stability
Concentration of slurry (0.5–50%)			
Nozzle size of equipment (0.5–1.5 mm)			
Binder content (0–50%)			
Drying temperature (60–150 °C)			
Compressor pressure (0.1–2 bar)			
Sample flow (1–50 mL min ⁻¹)			
Air flow (20–70 m ³ h ⁻¹)			
Primary particle size (9–750 nm)			
Polarity of solvent (EtOH, MeOH and water)			

The range of values for each parameter is given in brackets.

by the low specific pore volumes of agglomerates produced from these materials.

2.1.2. Morphology of agglomerated colloids

The pre-agglomerated Aerosil nanoparticles produced perfectly spherical agglomerates, whereas agglomeration of non-agglomerated Levasil and M25 sols resulted in collapsed spheres possessing single perforations (see Fig. 4). These structures have been previously described as “donuts” in literature [25–27]. Interestingly, when M250 and M500 dis-

persions were spray dried, the morphology of the agglomerates was spherical (see Fig. 5). However, these agglomerates were not stable enough to be used in our application, and disintegrated during the MAO impregnation procedure, as observed by SEM. This behaviour can be explained with the much lower ratio R of secondary particle size to primary particle size in the case of spray dried M250 and M500 compared to M25; at a fixed secondary particle size of 10 μm, the R -values were 40, 20 and 400 for M250, M500 and M25 primary particles, respectively. In addition, one has to take

Table 3

Morphological (SEM-derived) and pore structure (derived from nitrogen sorption) data on the colloidal systems following spray drying

Starting binder material	Morphology	Specific surface area, a_s (BET) (m ² g ⁻¹)	Specific pore volume, v_p (G) (mL g ⁻¹)	Mean pore diameter, p_d (BJH _{des}) (nm)
Levasil 50	Donuts	48.1	0.27	18.8
Levasil 100	Donuts	127.0	0.21	5.8
Levasil 200	Donuts	162.1	0.16	3.7
Levasil 300	Donuts	235.5	0.15	2.5–3.5
Levasil 50S1	Donuts	33.2	0.31	36.0
Levasil 50S2	Donuts	22.3	0.32	60.0
Aerosil 90	Spheres	86.7	1.46	95.4
Aerosil 200	Spheres	180.4	1.93	56.8
Aerosil 300	Spheres	289.1	1.99	36.0
M 25	Donuts	286.4	0.21	3.7
M 250	Spheres	12.6	0.21	100
M 500	Spheres	6.1	0.22	200

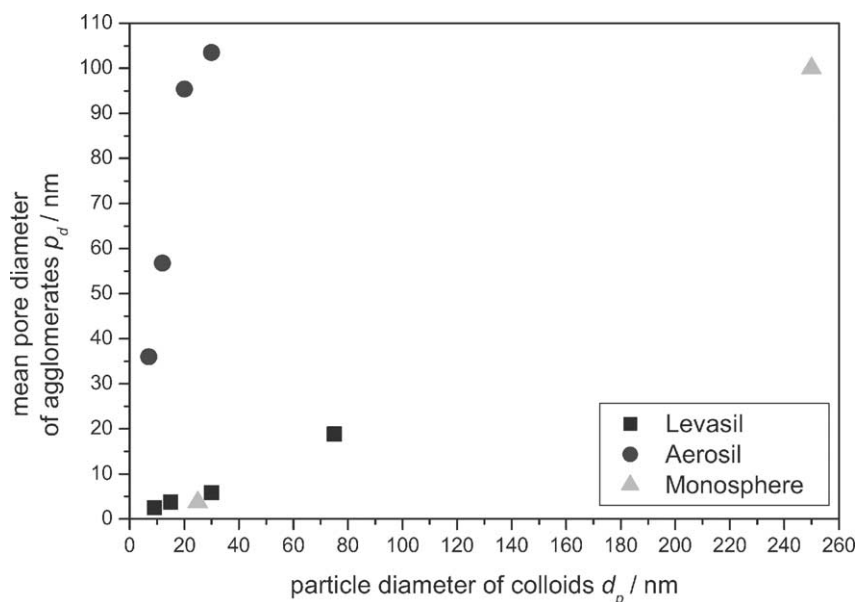


Fig. 3. Dependence of the particle size on the mean pore diameter of Levasil, Aerosil and Monosphere colloids following agglomeration.

into account the significant role of specific surface area in determining the agglomerate strength, and the fact that the surface area was decreasing with increasing primary particle size.

In order to create a model carrier, we combined the favourable spherical morphology of the agglomerated M250 and M500 with colloids having particle dimensions below 100 nm.

2.1.3. Impact of the nature and percentage of colloids on the porosity and morphology of agglomerated M250 and M500

Dispersions of M250 and M500, respectively, were spray dried following the addition of the colloids presented in Table 3 in order to assess the pore structural and morphological changes in comparison to the purely agglomerated M250 and M500 particles. The smaller colloids, which acted

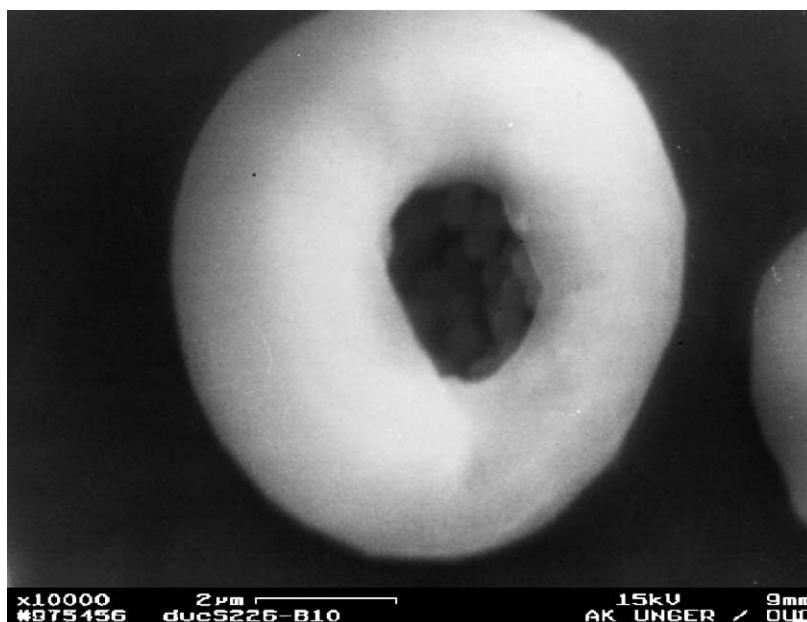


Fig. 4. Example of the “donut” morphology obtained by spray agglomeration.

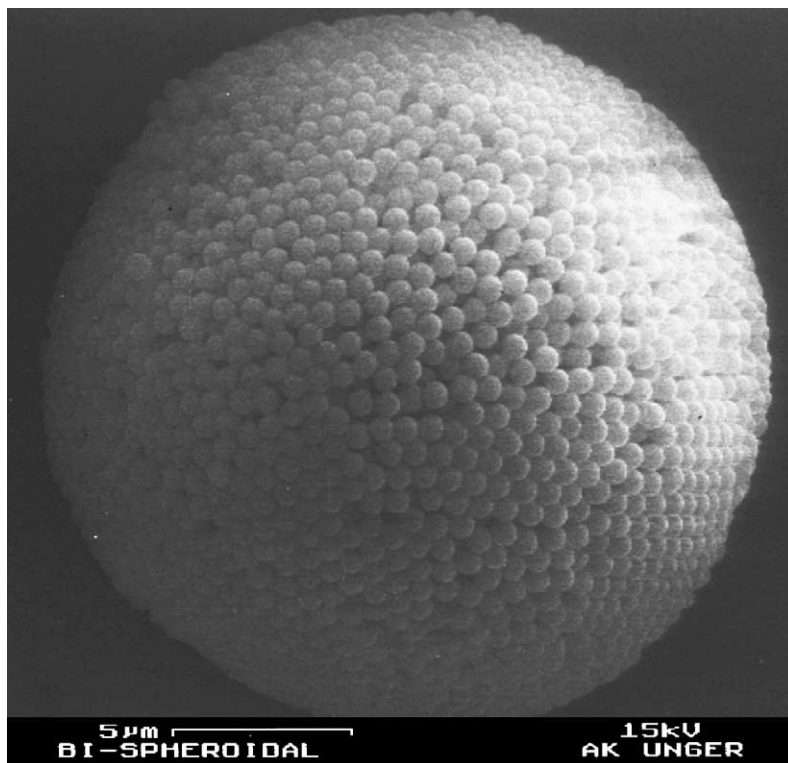


Fig. 5. SEM image of a spherical agglomerate consisting of 500 nm monodisperse non-porous silica spheres.

as binders, were added to the dispersion at concentrations of up to 35 wt.%. As can be seen from Figs. 6 and 7, the specific surface area generally increased with increasing binder percentage. The slope of this dependence, however, was different for each binder system. It can be clearly seen that a plateau was reached at low binder contents with most colloids. Only M25 gave a steep slope resulting in much higher specific sur-

face areas of the agglomerates compared to the other binders at similar contents. Thus, the surface area could be best tuned using M25 as binder material.

Scanning electron microscopy was used to investigate the morphology of the agglomerates. The purely agglomerated Levasil sols possessed the aforementioned “donut” morphology. However, in the presence of M250 and M500, the re-

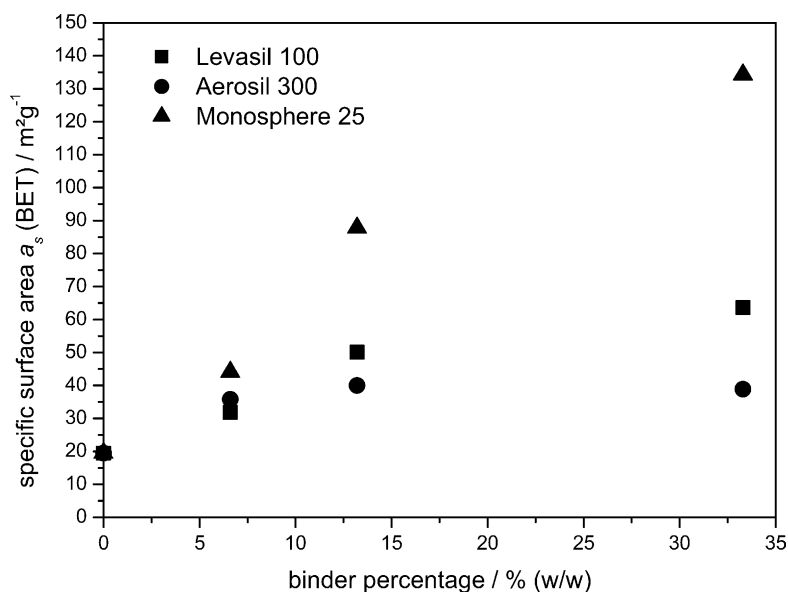


Fig. 6. Specific surface areas, derived from nitrogen sorption experiments, of agglomerated M250 vs. binder type and content.

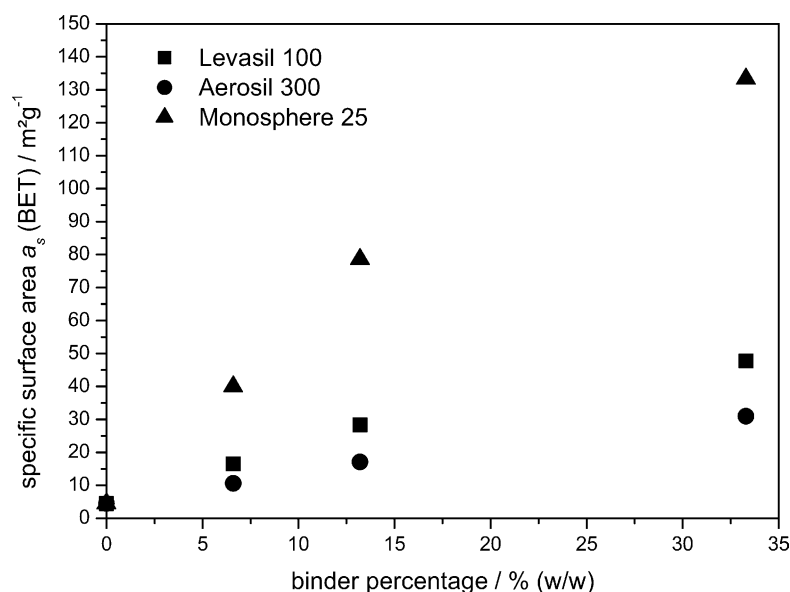


Fig. 7. Specific surface areas, derived from nitrogen sorption experiments, of agglomerated M500 vs. binder type and content.

sulting agglomerates were changed from spherical particles, at Levasil concentrations of 0–9 wt.%, to donut-shaped particles, starting from a critical concentration of 9 wt.%, as documented in Fig. 8A–C. In the case of agglomerated M250/M25 and M500/M25, no change in morphology was observed even at high M25 concentrations (33 wt.%). The SEM pictures (Fig. 9A–C) show the formation of a thin layer of M25 with increasing concentration, maintaining the perfectly spherical morphology and stabilising the agglomerate. One reason for this behaviour could be the similar surface properties of the M25, M250 and M500 materials, which might lead to a more homogeneous distribution of the M25 binder particles in comparison with the Levasil type, which are stabilised with electrolytes [28].

2.2. Characterisation of the model agglomerate carrier systems

As indicated in the previous chapter, the combination of M250 and M500 primary particles with M25 binder particles led to model carriers with well-defined and homogeneous morphological, geometrical and pore structural properties.

The M250/M25 and M500/M25 carrier systems are made up of two discrete sizes of silica particles which create a bimodal pore size distribution in the agglomerates, with the pore network consisting of interstitial voids between the pri-

mary and the binder particles. A schematic of the model agglomerate is given in Fig. 10.

As shown in Fig. 11, it was possible to detect both pore diameters by nitrogen sorption, although the larger pores were situated in the lower macropore size range, rendering this method less accurate. Nevertheless, the isotherms of both systems were characterised by a flat slope at low relative pressures, typical of non-porous materials. The bimodal pore size distribution curves in Fig. 11 reflected the two separately observed hystereses in the desorption branch of the isotherms, with each hysteresis corresponding to a distinct pore size distribution. Comparing the M250/M25 and M500/M25 systems, it became clear that each particle size, i.e. 25, 250 and 500 nm, built up its own pore network. Mercury intrusion experiments (Fig. 12) confirmed this hypothesis. Table 4 summarises the calculated pore diameters for each particle dimension. The average coordination numbers of the particles within the densely packed agglomerates are also given. These values were estimated according to geometrical considerations [29] and show good agreement between both methods. In conclusion, the agglomerated carriers represent relatively dense-packed agglomerates of monodisperse silica spheres with high coordination numbers.

According to theory, the maximum amount of the binder that can be accommodated within the interstitial space of the primary particles varies with the type of packing. Fig. 13

Table 4

Mean pore diameters and coordination numbers of agglomerated M25, M250 and M500, as measured by nitrogen sorption and mercury intrusion

Particle diameter, d_p (nm)	Mean pore diameter, p_d (nm)		Mean co-ordination number (n)
	Nitrogen sorption (BJH_{des})	Mercury intrusion	
25	3.7 ($0.15d_p$)	5.5 ($0.22d_p$)	12
250	100 ($0.40d_p$)	100 ($0.40d_p$)	9
500	200 ($0.40d_p$)	200 ($0.40d_p$)	9

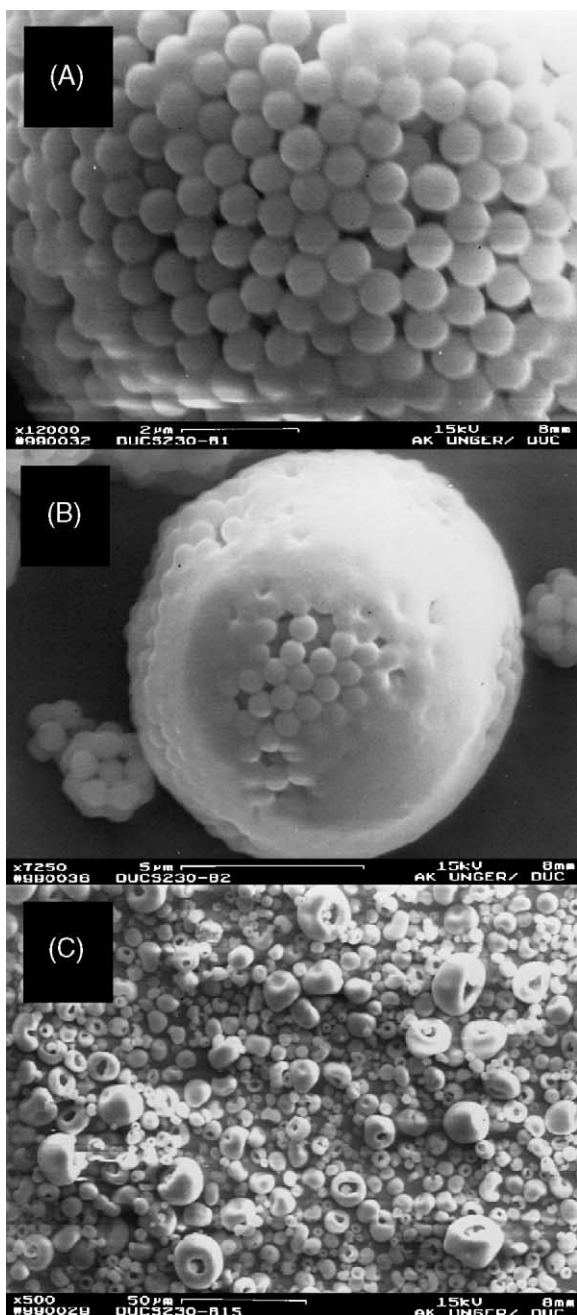


Fig. 8. SEM images of M500 agglomerates with increasing binder content: (A) 3 wt.%; (B) 6 wt.%; (C) 9 wt.%; Levasil 100 binder.

shows that the maximum calculated binder percentage was found to be around 20% when the experimentally assessed coordination numbers from Table 4 were considered. The fact that significant skin formation took place with an M25 concentration higher than 20 wt.% (Fig. 9A–C) gives direct experimental proof for this conclusion.

Binder percentages of 8, 20 and 33 wt.% were, therefore, chosen for the production of model carriers in order to cover a range of binder concentrations around the critical binder concentration.

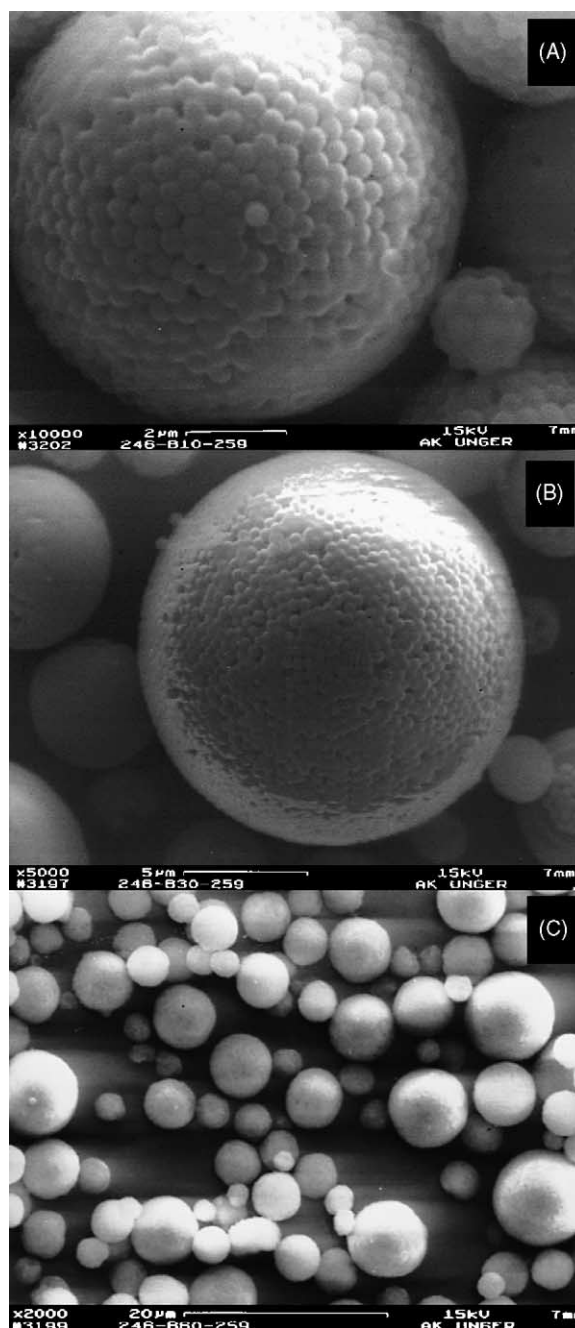


Fig. 9. SEM images of M500 agglomerates with increasing binder content: (A) 8 wt.%; (B) 20 wt.%; (C) 33 wt.%; Monospher M25 binder.

2.3. Carrier treatment prior to polymerization

Various concepts for heterogenization of the catalyst system are discussed in the literature [30–33]. We chose the well-established approach of first impregnating the carrier with MAO, then reacting it with the metallocene [34,35].

In a heterogeneous polyethylene polymerization, the polymer serves as a matrix for the carrier. The carrier is broken up during polymerization by the increasing hydraulic pressure arising from the growing polymer chains, leaving behind

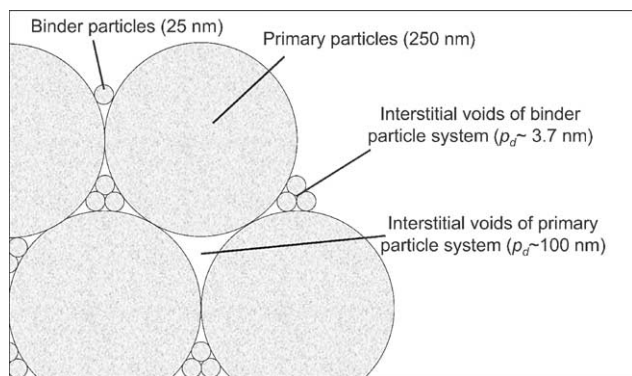


Fig. 10. Schematic representation of the model carrier system and its pore architecture.

fragments that will influence polymer properties like mechanical behavior and film formation characteristics. Therefore, it is extremely important to obtain a catalyst system where the active sites are evenly distributed and not simply immobilised at the outer surface of the carrier. This was checked by scanning electron microscopy (SEM) coupled with energy-dispersive X-ray analysis (EDX) of the agglomerated silica carriers following MAO impregnation. Fig. 14 shows the spatial distribution of oxygen, silicon, carbon and aluminium in the interior of the carrier following microtoming to expose the interior of the carrier particles (slices were $\sim 2 \mu\text{m}$ in thickness, carrier was embedded in a PMMA matrix). The homogeneous dispersion of the aluminium, corresponding to the MAO co-catalyst, is readily observed. Silicon and oxygen (from the silica particles themselves) and carbon (from the PMMA embedding medium), are also observed.

The influence of MAO impregnation on the pore structure of the carriers was investigated by nitrogen sorption measure-

ments. The adsorption/desorption isotherms of the MAO-impregnated agglomerates (Fig. 15) indicate a decrease in specific surface area and specific pore volume of approximately 25%. The observed decrease stems from the fact that considerable amounts of MAO were introduced, causing a density increase, as expected. Fig. 16 reveals that the mesopore system was still detectable following MAO impregnation, meaning that the mesopores remained accessible following grafting of the co-catalyst.

2.4. Slurry polymerization of ethylene

The agglomerated silicas M250/M25 and M500/M25 with varying M25 content were employed as carriers in the heterogeneous polymerization of ethylene using MAO as the co-catalyst and dicyclopentadienyl zirconium dichloride as the pre-catalyst species. Triisobutylaluminum (TIBA) was employed as a scavenger. The polymerization reaction was stopped after 1 h and the polymer yield was calculated after drying at 100°C . The results are shown in Fig. 17, where the polymerization activity A ($\text{kg}_{\text{PE}}/\text{mol}_{\text{cat}} \text{ h bar}_{\text{ethylene}}$) is plotted versus the binder content in both systems.

3. Discussion

3.1. Polymerization activity

The results of the polymerization activity are summarized in Table 5. The highest polymerization activity for the M250/M25 system was found with the lowest M25 content (carrier 1a). Increased binder content resulted in reduced activity. In contrast, the highest catalytic activity in

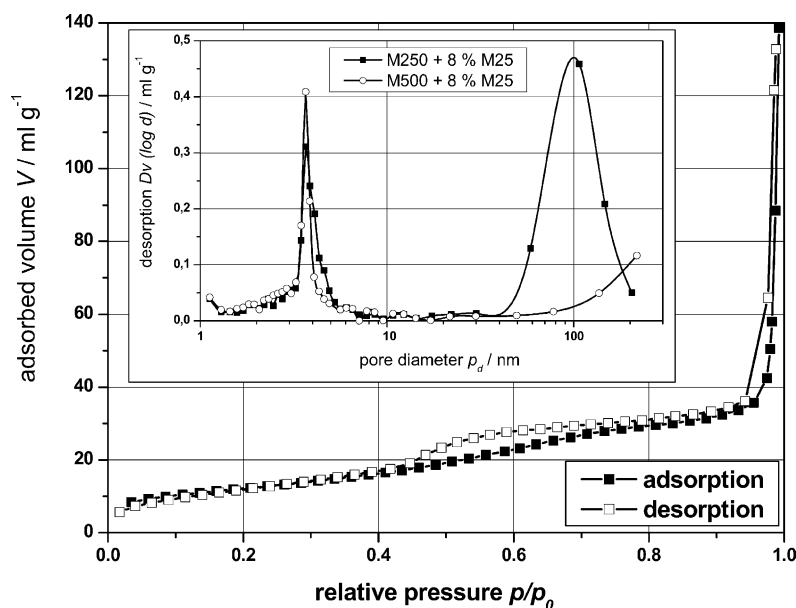


Fig. 11. Nitrogen sorption isotherm of carrier 1a and pore size distributions (inset) of carriers 1a and 2a, as calculated by the BJH method.

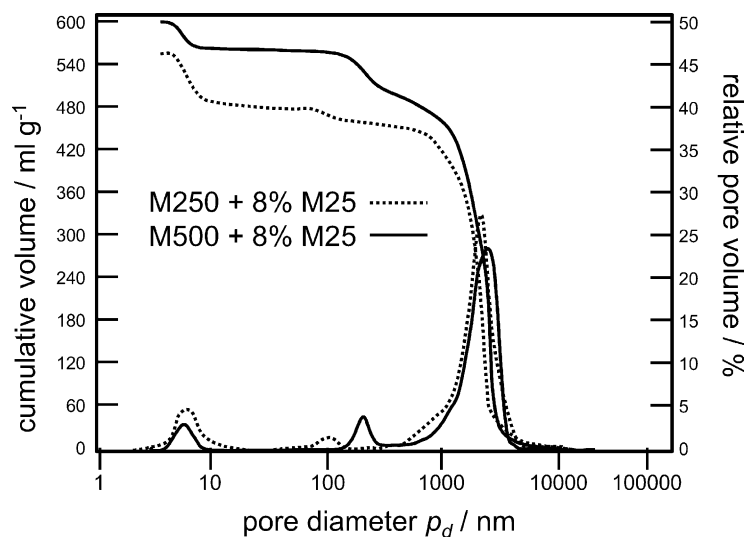


Fig. 12. Pore size distributions of agglomerated M250 and M500 with 8 wt.% M25 (carriers 1a and 2a), as calculated from mercury intrusion measurements.

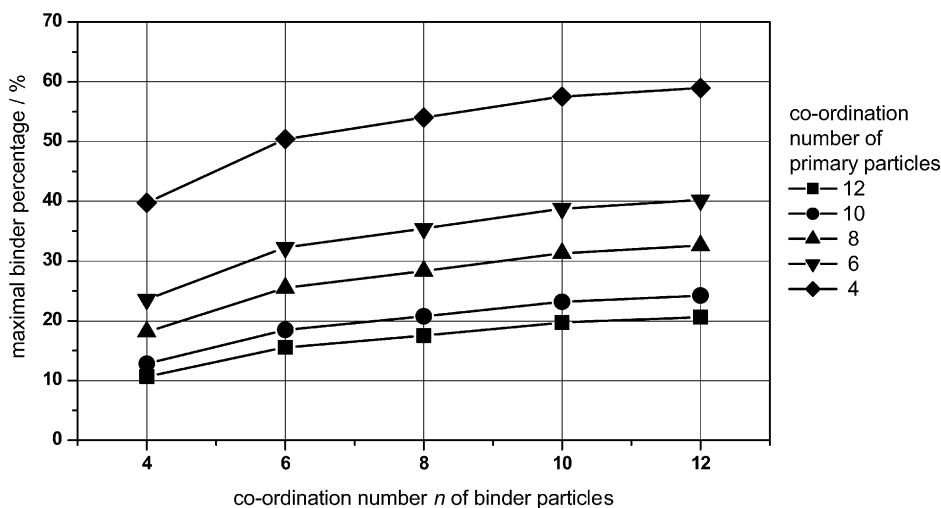


Fig. 13. Calculated maximal binder content, based on the coordination number of binder and primary particles.

the M500/M25 system was observed with 20 wt.% binder (carrier 2b). Deviations from this binder content resulted in reduced activity. With increasing percentage of binder, the specific surface area was enlarged in both systems. As the surface area values were similar for both systems for

equal M25 concentrations, it was deduced that the surface area was mainly determined by the M25 particles, whereas the contribution of the primary particles, i.e. M250 and M500, was negligible. In our model systems, however, the polymerization activity was not proportional to the spe-

Table 5
Carrier and polymer properties of investigated carrier systems

Carrier no.	Carrier system	Specific surface area, a_s ($\text{m}^2 \text{g}^{-1}$)	Polymerization activity, A ($\text{kgPE} (\text{mol}_{\text{cat}} \text{h bar}_{\text{ethylene}})^{-1}$)	Molecular weight, M_w (g mol^{-1})	Poly-dispersity (M_w/M_n)	Melting point, T_M ($^\circ\text{C}$)	Crystallinity (%)
1a	M250 + 8% M25	44.1	392	373.000	3.5	140.8	61.0
1b	M250 + 20% M25	87.8	131	710.000	4.4	139.3	41.5
1c	M250 + 33% M25	134.3	79	875.000	3.1	136.5	37.4
2a	M500 + 8% M25	40.0	68	746.000	3.2	137.8	32.5
2b	M500 + 20% M25	78.6	340	593.000	4.2	139.8	56.6
2c	M500 + 33% M25	133.3	62	700.000	3.8	138.2	33.7
3	SYLOPOL 948	295.6	374	420.000	2.5	–	–

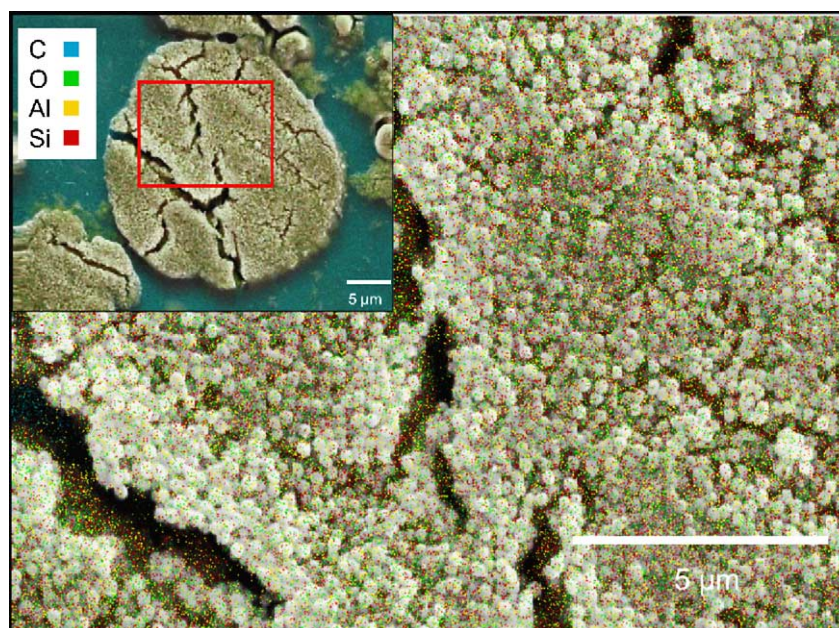


Fig. 14. SEM–EDX derived elemental map of carrier 1a after impregnation with MAO.

cific surface area of the carriers, meaning that the total quantity of catalytic sites distributed on the surface was not the determining factor with respect to overall carrier activity.

Care was taken, during carrier treatment, to ensure complete saturation of the agglomerate surface with MAO. This was verified from elemental analysis for aluminium, via atom absorption spectrometry of the washing solutions following MAO impregnation (data not shown). Therefore, the differences in catalytic activity cannot be attributed to variations in MAO content.

For reasons of comparison the catalytic activity of a commercially available carrier Sylopol 948 (W.R. Grace) was investigated, using the same carrier pre-treatment procedures

and polymerization conditions. The activity of Sylopol 948 (see Table 5) was comparable to that of the agglomerated carriers 1a and 2b, although its specific surface area was 4 to 8 times higher than our systems.

3.2. Polymerization activity—structure relationship between polymer and carrier properties

In addition to the effect of the pore structure, the binder content also affected the mechanical stability of the agglomerated colloidal silicas. Specifically, the mechanical stability of our agglomerates was proportional to the binder content, due to the formation of a dense surface layer of binder particles with increasing binder content (see Fig. 9B and C).

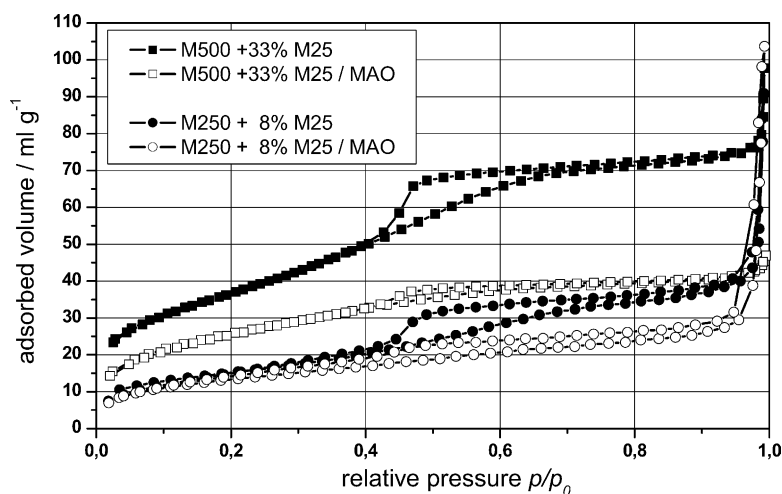


Fig. 15. Nitrogen sorption isotherms of agglomerated carriers 1a and 2c with M25 as binder before and after impregnation with MAO.

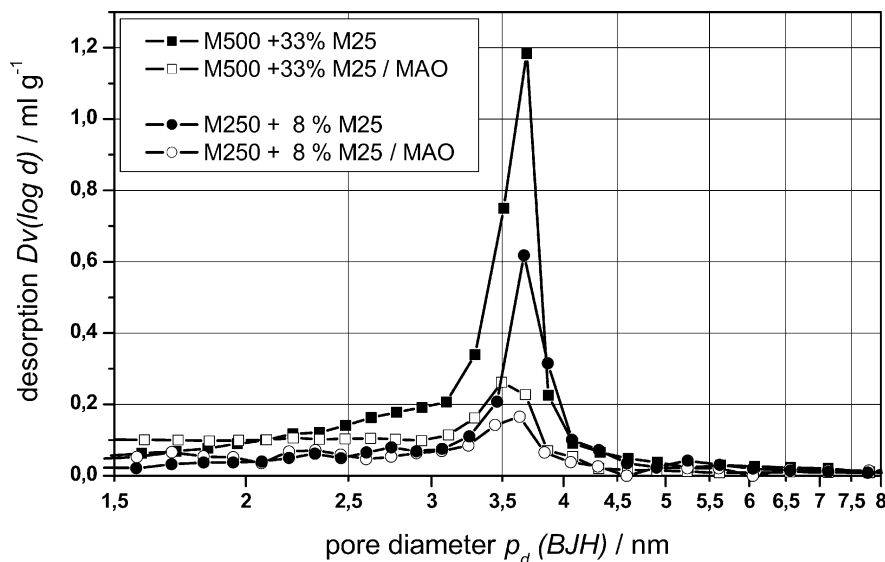


Fig. 16. Pore size distributions of carriers 1a and 2c (calculated according to the BJH-method) before and after impregnation with MAO (shown range: 1.5–8 nm).

In the same fashion, the specific surface area also increased with increasing binder content, implying an increased number of reactive surface silanol groups available for bridging and condensation. The agglomerate strength of the carriers was an important aspect in this study, as in terms of polymerization, it determined the particle fragmentation behaviour, and thus the time necessary for the olefin monomer to reach all active sites within the carrier agglomerates.

In the M250/M25 system, with increasing agglomerate strength, the carriers with 20 and 33 wt.% binder, respectively, showed low catalytic activities. From data on the extent of polymerization, where the different stages of polymerization could be identified (data not shown), and from morphological studies (via SEM), we conclude that

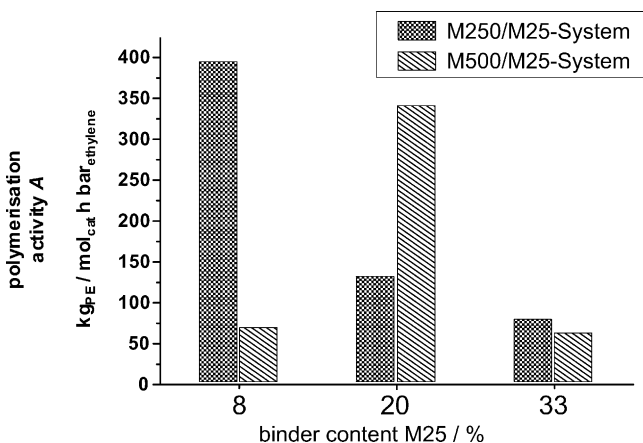


Fig. 17. Polymerization activity of carrier systems 1a–c and 2a–c vs. binder content. Polymerization conditions: 0.5 g carrier, 5.4 mmol MAO, 4.3 μ mol Cp_2ZrCl_2 , 0.4 mmol TIBA, 2.5 bar ethylene, 115 mL toluene, 1 h polymerization, begun at room temperature (see Section 5).

the carriers were too stable to break-up. Fragmentation did not occur within the recorded time frame. The M500/M25 system showed the best polymerization activity with a binder content roughly twice as high as in carrier 1a. As the primary particle size was doubled, one might expect that carriers 1a and 2b should have similar mechanical properties, representing an optimum value for the studied polymerization process. Lower binder contents gave extremely fragile agglomerates that broke up under magnetic stirring during the carrier pretreatment. This was confirmed by SEM in the case of carrier 2a (Fig. 18). Clearly, the agglomerated M500 particles have lost their spherical super-structure and the agglomerates have disintegrated. Due to the high dispersion of the carrier 2a within the polyethylene product after polymerization, it was impossible to study agglomerate behaviour via SEM.

Agglomerates with higher binder contents were characterised by a dense layer of binder particles at the surface, giving increased mechanical stability. In addition to this effect, it should be remembered that the interstitial voids of the primary particles were almost completely filled with the binder at 20 wt.% of binder (according to Fig. 13). The resulting diffusion barrier contributed to the suppression of the fragmentation and the extension of the induction period. SEM results (Fig. 19) show that the morphology of the “rigid” carrier 2c remained nearly unchanged following polymerization, supporting the aforementioned arguments (compare with Fig. 9C).

Table 5 shows that for both carrier systems high polymerization activity resulted in lower molecular weights. This suggests that the polymerization with carriers 1a and 2b are highest due to the largest number of catalytic sites accessible to the monomer, thus producing shorter polyethylene molecules. This feature is reflected in the DSC data where

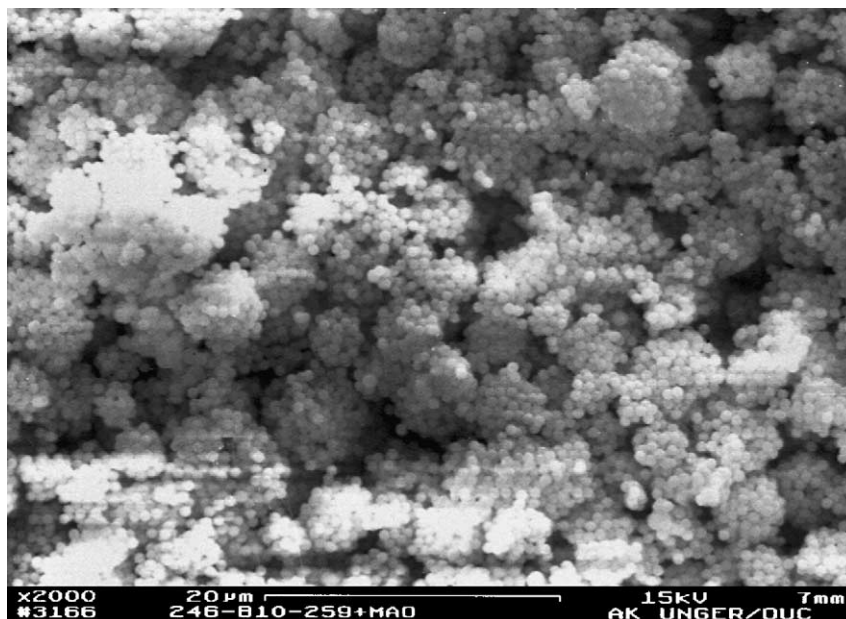


Fig. 18. SEM image of carrier 2a following impregnation procedure with MAO (see Section 5).

higher melting points of the polyethylene samples were observed for the most active carriers 1a and 2b. An explanation could be the lower degree of entanglement that is possible in shorter PE chains in comparison to longer PE. This assumption is confirmed by the crystallinity data obtained with a reference PE in DSC. The measured crystallinity decreased

with decreasing melting point and was found to be highest for the most active carriers.

Comparing the molecular weights of our samples with commercial carrier 3, we found similar values and, in general, the presented data indicate that high-density polyethylene (HDPE) had been produced in all cases.



Fig. 19. SEM image of polyethylene product following polymerization with carrier 2c. Polymerization conditions: 0.5 g carrier, 5.4 mmol MAO, 4.3 μmol Cp_2ZrCl_2 , 0.4 mmol TIBA, 2.5 bar ethylene, 115 mL toluene, 1 h polymerization, begun at room temperature (see Section 5).

4. Conclusions

Spherical agglomerates possessing bimodal pore size distributions arising from interstitial voids between two different-sized non-porous and monodisperse silica spheres, i.e. the primary and the binder particle were synthesised. The appropriate combination of primary particles (M250 and M500) and binder particles (M25) was chosen according to morphological studies indicating the desired morphology (spherical particles) and porosimetry analyses indicating the desired pore structure (uniformly narrow pore size distributions, and high particle coordination numbers). The resulting model agglomerates were employed as carriers in the heterogeneous polymerization of ethylene using MAO as the co-catalyst. The MAO was evenly distributed within the carriers and adsorption data indicate no pore-blocking following the immobilisation procedure. The effects on the catalytic activity, the extent of polymerization, and the polymer properties were studied with carriers comprising different primary particle sizes, i.e. 250 nm/25 nm and 500 nm/25 nm, with increasing percentage (8–33 wt.%) of the 25 nm binder particles. With respect to catalytic activity, optimal binder concentrations were found to be 8 wt.% in the case of the M250/M25 system and 20 wt.% in the case of M500/M25 system. The mechanical stability of the carriers, as influenced by its binder content, and the fragmentation of the carriers during slurry polymerization, were evaluated via SEM. A comparison with a commercial silica carrier (Sylopol 948), utilized under equivalent conditions, revealed that similar catalytic activity was found in our model systems, despite the fact that their surface areas were up to eight times lower than that of the commercial carrier.

5. Experimental

5.1. Agglomeration

A suspension of primary particles was prepared by adding 6 g of Monospher silica (250 or 500 nm, respectively) to 100 mL of deionised water prior to ultrasonic treatment (20 min). The suspension was magnetically stirred for 30 min using a Teflon-coated magnetic stir. Following addition of the binder solution (10 wt.% 25 nm Monospher silica), the suspension was spray dried immediately using a Labplant LP SD 05 spray-drier. The spray drying parameters were as follows: air temperature = 120 °C; air velocity = 15 (relative); flow velocity = 10–12 mL/min; compression pressure = 0.5–0.8 bar; nozzle inner diameter = 1.0 mm.

5.2. Polymerization of ethylene

5.2.1. Equipment and procedures

The preparation of the co-catalyst/carrier system was conducted under an inert gas atmosphere (argon, 6.0 grade). Toluene was dried over sodium and introduced to the reaction

vials and the reactor via the Schlenk technique. All containers were evacuated and purged with argon using a standard vacuum line.

5.2.2. Impregnation of the carriers with the co-catalyst MAO

Spray-dried silica carrier (0.5 g) were introduced into a 100 mL three-neck flask. Freshly dried toluene (35 mL) and 3.25 mL of methylaluminoxan solution (MAO, 10% in toluene, Aldrich) were added to the silica. The suspension was magnetically stirred with a Teflon-coated magnetic stir bar for 30 min, then allowed to sediment. The surplus toluene was removed via a filtration capillary equipped with a membrane filter (TE 35; 0.2 µm; Schleicher and Schuell) and the silica was then re-suspended with 5 mL dry toluene and filtered again.

5.2.3. Polymerization

The agglomerate carrier/MAO system was re-suspended in 40 mL dry toluene and 0.12 mL triisobutyl aluminum solution (TIBA, 0.24 µmol, 25% in toluene, Aldrich) was added. After a short period of stirring, the suspension was transferred to the polymerization reactor (Miniclave Drive, 250 mL reactor, Büchi), which was secured prior to all experiments. This procedure was repeated for complete transfer of the impregnated carrier. After a final addition of 15 mL of fresh toluene, 5 mL of a solution of the pre-catalyst, bis(cyclopentadienyl) zirconium dichloride, was introduced (10 mg in 40 mL of toluene). The mixture was stirred at 200 rpm, and after 10 min, the polymerization was initiated with ethylene (2.5 bar, 4.5 grade). The reactor temperature was monitored using a high-precision thermocouple (Testo 945). After 60 min, the polymerization was stopped via the addition of 400 mL of methanol/2 N HCl (50:50 (v/v)) and the polyethylene was filtered, dried and weighed.

5.3. Characterisation

Adsorption and desorption isotherms were measured at 77.4 K on a Quantachrome Autosorb 6B (Quantachrome Corporation, Boynton Beach, FL, USA) using nitrogen. The samples were out-gassed at 423 K and 1 mPa for 14 h before adsorption measurements.

Specific surface area was calculated according to the multipoint Brunauer, Emmet and Teller (BET) method, using the linear p/p_0 range (0.1–0.2) of the adsorption branch. The specific pore volume was calculated according to Gurwitsch at a p/p_0 -value of 0.975 of the desorption branch. The mean pore diameter was calculated according to Barret, Joyner and Halenda from the desorption branch of the isotherm (BJH desorption method). A cylindrical pore shape was assumed in the calculations.

Scanning electron micrographs were obtained using a Zeiss DSM 962 scanning electron microscope (Zeiss, Jena, Germany). Samples were attached to the sample holder using adhesive carbon tape and sputtered with gold.

Mercury intrusion measurements were conducted on a Porosimeter 2000 (Carlo Erba Instruments). The Washburn equation was used to calculate pore sizes and pore size distributions.

Polymer molecular weights were determined using a high-temperature GPC (Knauer), operated at 135 °C with 1,2,4-trichlorobenzene as solvent and the following conditions: injection volume = 400 µl; sample concentration = 0.5 mg/mL; flow = 1 mL/min; using polystyrene columns with a 50 to 10,000 nm range.

Polymers melting points were characterised via differential scanning calorimetry using a DSC-821 (Mettler Toledo). A reference PE was used for crystallinity determination.

Acknowledgment

The authors would like to express their thanks to Dieter Lubda (Merck KGaA) for helpful discussions, Kai Schumacher (Degussa AG) for supplying the Aerosil samples and Lothar Puppe (H.C. Starck GmbH) for supplying the Levasil samples.

References

- [1] G. Fink, R. Mülhaupt, H.H. Brintzinger (Eds.), *Ziegler Catalysis*, Springer-Verlag, Berlin, 1995.
- [2] W. Kaminsky, *Catalysis Today* 62 (2000) 23–34.
- [3] E. Albizzati, M. Galimberti, *Catalysis Today* 41 (1998) 159–168.
- [4] M.-J. Brekner, B. Bachmann, F. Osan, K. Alberti, A. Winter, *Chem. Abstr.* 122 (1995) 134–148.
- [5] J. Chowdhury, S. Moore, *Chem. Eng.* 100 (4) (1993) 34.
- [6] J. Baker, *Eur. Chem. News* 60 (1590) (1993) 22.
- [7] R. Mülhaupt, F. Stricker, *Kunststoffe* 87 (1997) 482.
- [8] P. Walter, D. Mäder, P. Reichert, R. Mülhaupt, *J. Macromol. Sci. A36* (1999) 1613.
- [9] P. Dubois, M. Alexandre, R. Jérôme, *Macromol. Symp.* 194 (1) (2003) 13.
- [10] M. Kaminaka, K. Soga, *Macromol. Rapid Commun.* 12 (1991) 367.
- [11] L.K. Van Looveren, D.E. De Vos, K.A. Verduyck, D.F. Geysen, B. Janssen, P.A. Jacobs, *Catal. Lett.* 56 (1) (1998) 53.
- [12] S.I. Woo, Y.S. Ko, T.K. Han, *Macromol. Rapid Commun.* 16 (1995) 489–494.
- [13] J.S. Bergman, H. Chen, E.P. Giannelis, M.G. Thomas, G.W. Coates, *Chem. Commun.* (1999) 2179–2180.
- [14] B. Steinmetz, J. Zechlin, C. Przybyla, B. Tesche, G. Fink, *Nachrichten aus der Chemie* 48 (2000) 12–17.
- [15] R. Goretzki, G. Fink, B. Tesche, B. Steinmetz, R. Rieger, W. Uzick, *Polym. J. Sci. A: Polym. Chem.* 37 (1999) 677–682.
- [16] G. Fink, B. Steinmetz, J. Zechlin, Chr. Przybyla, B. Tesche, *Chem. Rev.* 100 (2000) 1377–1390.
- [17] C.J. Brinker, G.W. Scherer, *Sol Gel Science*, Academic Press, 1990.
- [18] W. Stöber, A. Fink, E. Bohn, *J. Colloid Interface Sci.* 26 (1968) 62–69.
- [19] H. Giesche, *Diplomarbeit*, Johannes Gutenberg-Universität Mainz, 1983.
- [20] H. Giesche, *Dissertation*, Johannes Gutenberg-Universität Mainz, 1987.
- [21] A.P. Karnaukhov, *Kinet. Catal. (Russ.)* 12 (1971) 1025–1033.
- [22] R.G. Avery, J.D.F. Ramsay, *J. Colloid Interface Sci.* 42 (1973) 597.
- [23] S.E. Pratsinis, *Prog. Energy Combust. Sci.* 24 (1998) 197–219.
- [24] H.K. Kammiller, R. Mueller, O. Senn, S.E. Pratsinis, *AIChE J.* 47 (7) (2001) 1533–1543.
- [25] S.J. Lukasiewicz, *J. Am. Ceram. Soc.* 72 (1989) 617–624.
- [26] A.W. Adamson, *Physical Chemistry of Surfaces*, Wiley, New York, 1976.
- [27] K.J. Konsztowicz, G. Maksym, T. Maksym, H.W. King, W.F. Caley, E. Vargha-Butler, *Forming Sci. Technol. Ceram.* 26 (1990) 46–53.
- [28] Levasil product information sheet, Bayer AG.
- [29] R.G. Avery, J.D.F. Ramsay, *J. Colloid Interface Sci.* 42 (1973) 597.
- [30] J.C.W. Chien, D. He, *J. Polym. Sci. A: Polym. Chem.* 29 (1991) 1603–1607.
- [31] S. Collins, W.M. Kelly, D.A. Holden, *Macromolecules* 25 (1992) 1780–1785.
- [32] K. Soga, M. Kaminaka, *Macromol. Chem.* 194 (1993) 1745–1755.
- [33] W. Kaminsky, F. Renner, *Makromol. Chem. Rapid Commun.* 14 (1993) 239.
- [34] W. Kaminsky, D. Arrowsmith, C. Strübel, *J. Polym. Sci. A: Polym. Chem.* 37 (1999) 2959.
- [35] W. Kaminsky, H. Winkelbach, *Top. Catal.* 7 (1999) 61.